Egypt. J. Chem. **Vol. 65,** No. 9 pp. 639 - 655 (2022)

Egyptian Journal of Chemistry

http://ejchem.journals.ekb.eg/

Divalent transition metal complexes of multidentate nitrogen, oxygen and sulfur containing ligand: Design, spectroscopic, theoretical molecular modeling and antioxidant like activity

Bassam M. Ismael[1], Mohamed A.El_nawawy[1], Hosni A. Gomaa [1], Ola A. El-Gammal[2]*

[1] Chemistry Department, Faculty of Science, Al-Azhar University, Nasr City-Cairo 11884, Egypt

[2]Faculty of Science, Chemistry Department, Mansoura University, Mansoura

Abstract

A novel thiosemicarbazide, 2,2'-(9,10-dihydro-9,10-ethanoanthracene-11,12-dicarbonyl) bis (N-allyl hydrazine-1-carbothioamide) (TSc) (1) was prepared and characterized by elemental analysis, IR, ^{1}H, $^{13}CNMR$, electronic and mass measurements. Metal complexes (2-4) were also prepared by reacting with acetate salts of Co^{2+}, $Ni^{2+}$and Cu^{2+} ions and characterized by elemental, spectral (IR, UV-vis., ESR (for Cu^{2+}), mass, molar conductivity and magnetic moments measurements. IR data indicated the TSc chelates, as neutral ON in the mononuclear Co (II) complex, binegative $O_2N_2S_2$ hexadentate in binuclear Ni (II) and Cu (II) complexes or as mononegative ON neutral chelate in keto-thione form binding one Zn atom from one arm and in enol-thione form binding the other Zn atom in the second arm). Zn^{2+} complex afforded a tetrahedral geometry while other complexes assigned an octahedral environment. The thermal degradation was studied to establish the thermal stability of the title compounds and the kinetic parameters were evaluated. Also, DFT method was used to draw the geometry of all compounds and the parameters such as bond lengths, bond angles, dipole moment, Frontier orbitals (HOMO, LUMO), MEP and other energetic parameters (optical energy gap, softness, hardness, electronegativity) were evaluated. Furthermore, the compounds were screened for DNA binding as well as SOD antioxidant activities.

Keywords: novel thiosemicarbazides, NMR, mononegative ON, energetic parameters and antioxidant activity.

Introduction

Compounds especially thiosemicarbazides that contain nitrogen, sulfur and or oxygen have gained significant interest in chemistry due to their wide pharmacological properties such as antiparasital [1], antibacterial [2], antitumor [3], antimalarial [4], antineoplastic [5] and antivira1 [6, 7]. The antitumor activity of some thiosemicarbazides derivatives was enhanced by forming specific metal ion chelates [8]. The thiosemicarbazides antiviral activity originated from inactivation of ribonucleotide reductases that are vital for viral replication [9]. Thus, thiosemicarbazide structural modification have done to find more effective chemotherapeutic agents [10]. Cobalt, like nickel, has variety of oxidation states and has more than five 3d-electrons in its lower oxidation state, i.e. acts as electron rich. Cobalt and nickel 3d electrons are forced into exposed σ- or π-orbitals in these low-spin states which means that it acts as active free radical like in case of vitamin B12. The vitamin B12 structure, anti-pernicious anemia factor, is an alkyl-cobalt (III) complex of a substituted corrin in which the sixth ligand is a 5'-deoxyadenosyl group. Many reactions that use the B12 coenzyme take place by free-radical pathways initiated or catalyzed by homolytic cleavage of the Co–C bond to form a Co(II) species and a deoxyadenosyl radical [11] Copper is an essential trace mineral necessary for survival. It is found in all body tissues and plays a role in making red blood cells and maintaining nerve cells and the immune system. It also helps the body form collagen and absorb iron, and plays a role in energy production. Copper is a vital and pertinent element for life [12]. It is one of the essential elements in most of the aerobic organisms and is employed as a structural and catalytic cofactor in a number of biological pathways [13 -15]. Copper ion

*Corresponding author e-mail: olaelgammal@yahoo.com, ORCID: 0000-0003-4119-7447

Receive Date: 26 January 2022, Revise Date: 21 March 2022, Accept Date: 28 April 2022

DOI: 10.21608/EJCHEM.2022.118264.5331

is potentially harmful due to its ability to engage in chemical reactions which generate hydroxyl radicals; a free radical species that directly damages deoxyribonucleic acid (DNA), proteins, and membrane lipids. So, the concentration of copper is tightly regulated at the level of cells, organs, and body of humans [16]. Copper nano films were found to be highly effective in growth inhibition of many nosocomial bacteria and Enterobacter species, and are used in touch surfaces in health care settings and hospitals to control germ proliferation [17,18]. The growth inhibition effect, called "contact killing" led to the approval of metallic copper as the first solid antimicrobial material by the United State Environmental Protection Agency (US EPA) [19].

The above aforementioned facts motivated us to prepare and characterize a series of Cobalt (II), nickel (II) and Copper (II) complexes derived from a multidentate selective thiosemicarbazide namely 2,2'-(9,10-dihydro-9,10-ethanoanthracene-11,12-dicarbonyl) bis (N-allyl hydrazine-1-carbothioamide) (TSc). The study included also the theoretical modelling using DFT method and the screening of the compounds as SOD like activity and DNA binding.

2. Experimental

2.1. Chemicals

All the chemicals used in the extraction and fractionation procedures were of analytical grade, obtained from Sigma-Aldrich (St. Louis, MO, USA), and used as received. HPLC-grade solvent was used for the GC-MS analysis.

2.2. Equipment

IR spectra were recorded on Jasco FTIR–4100 spectrophotometer FTIR spectra (KBr discs, 4000–400 cm^{-1}); ^{1} H NMR and ^{13}C NMR spectra were displayed using Bruker WP running at 300 and 80 MHz, respectively with using DMSO-d_6 as a solvent; Perkin-Elmer AA800 spectrophotometer Model AAS UV–visible spectra with a 1.0 cm cell model was used for displaying electronic spectra and evaluating DNA binding and SOD-like activities.The molecules were designed especially by Perkin Elmer ChemBio3D as software [25]. Thermal analysis data of the ligand and the complexes was achieved using a nitrogen atmospheric Shimadzu thermogravimetric analyzer with a rate of heating is 10 °C/min over a range of temperatures from temperature of room to 800 °C.

2.3. Synthesis of 2,2'-(9,10-dihydro-9,10-ethanoanthracene-11,12-dicarbonyl) bis(N-allylhydrazine-1-carbothioamide)

The thiosemicarbazone under investigation; TSc was prepared (Scheme 1) by heating the hydrazide (9,10-dihydro-9,10-ethanoanthracene-11,12-diacidhydrazide) [20] with allyl isothiocyanate (1:2) molar ratio under reflux for 5 hrs. A white precipitate (H_2TSc) was formed, filtered off, washed several times with ethanol and finally dried under vacuum in a desiccator over silica gel and checked by TLC and characterized by elemental analyses (C, H, N, S) (Table 1) and spectral (IR, Mass, 1H, 13CNMR and UV-vis.).

Yield: 85% (5.50 g) white; m.p.:265 0C; Elemental Anal. % Calc; C (59.97); H (5.42); N (16.14); S (12.31); Found: C 59.84;.H 5.49; N 15.94; S 12.10, FTIR:(Cm^{-1}): 3281 ν(N^1H); 3375 ν(N^4H); 3171 ν(N^2H); 1710;(C=O) $_{bonded}$; 1680(ν(C=O) $_{free}$; 1325 δ(C-H); 918 δ(N-H); 1290 ν(C=S); 799 δ(C=S); 1610 ν(C=C) $_{phenyl}$; 1021 ν(N-N);3060 $(CH)_{aromatic}$. UV-vis. in DMF (41322, 33500,28090); ^{1}HNMR (δ, ppm): 3.34 (dd, J = 3.6 Hz, 1H), 3.42-3.50 (m, 1H), 3.75 (s, 3H), 3.91 (s, 3H), 3.99-4.20; 5.03-5.12 two quartet signals ; two dd 3.07-3.63 and 3.70-4.12 and 4.27 (CH_2(-N^4H-CH_2) & CH_2(CH=CH_2); 6.98 (d, J = 9.0 Hz, 4H), 7.19-7.66 (m, 12H), N^1H 9.23 (d, 1H); N^2H 9.16 ; 7.77 N^4H

2.4. Synthesis of metal complexes

Hot ethanolic solution (20 ml) of the respective chloride salt, $CoCl_2.6H_2O$, $NiCl_2.6H_2O$ and $CuCl_2.2H_2O$ (0.001 mol) was added to a hot ethanolic suspension (20 ml) of the respective ligand (0.001 mol) with constant stirring and heating under reflux for 4 hrs. (Scheme 1) till a precipitate was formed, filtered off, washed several times with hot ethanol and dried under vacuum anhydrous $CaCl_2$.The physical and analytical data are listed in Table 1.

2.5. Biological activity

2.5.1.DNA binding assay

This assay [21] is based on the fact that methyl green binds to DNA in a reversible manner and that the coloured complex remains stable at neutral pH, whereas free methyl green fades at this pH. Active chemicals that bind to DNA displace DNA from its methyl green complex. A spectrophotometric experiment revealed the displacement as a reduction in absorbance at 630 nm. DNA methyl green (20 mg) was suspended in 100 ml of 0.05 M Tris-HCl buffer (pH 7.5) containing 7.5 mM $MgSO_4$; the mixture was stirred at 37 °C with a magnetic stirrer for 24 h. Test samples 10,100, 1000 mg) were dissolved in ethanol in Ependoff tubes, solvent was removed under vacuum, and 200µl of the DNA/methyl green solution were added to each tube. Samples were incubated in the dark at ambient temperature. After 24 h, the final absorbance of the samples was determined at 642.5-645 nm. Readings were corrected for initial absorbance and normalized as the percentage of the

untreated standard. The IC_{50} is a measure of how effective concentrations required for a 50% reduction in the initial absorbance of the DNA/methyl green solution were computed (mean SD, n= 3-5 independent determinations). The readings were normalized as a percentage of the untreated standard after being corrected for initial absorbance.

2.5.2. Superoxide dismutase (SOD) scavenging activity

The title compounds' SOD activity was measured using phenazen methosulfate (PMS), which photogenerated a consistent and repeatable flow of superoxide anion radicals at pH=8.3 (phosphate buffer) [22]. The reduction of nitroblue tetrazolium (NBT) to blue formazan was utilised as a spectrophotometric biomarker of O2-production at 560 nm. The addition of PMS (9.3 x 10^{-4}M) to an aqueous solution of NBT (3.0 x 10^{5} M), NADH (nicotine amide adenine dinucloted, 4.7 x 10^{-4}M), and phosphate buffer (final volume of 2 ml) resulted in a shift in OD(560)/ min[22]. For 3 minutes, the reaction was monitored in blank samples and in the presence of the chemicals under investigation. For comparative intents, the activity of *L-Ascorbic acid* has also been determined.

2.6. Molecular modeling

The cluster estimations [23] and double numerical basis sets plus polarisation functional (DNP) implemented in Materials Studio bundle [23] were investigated using DMOL3 module computations. It's made to carry out large-scale density functional theory (DFT) calculations [24, 25]. The geometric optimization is done without regard for symmetry.

3. Results and discussion

3.1. IR spectra

The significant assignments of IR spectral bands of the title thiosemicarbazide, TSC and its divalent complexes (as KBr discs) (Table 2) were elucidated by careful comparison with the spectrum of the hydrazide (9,10-dihydro-9,10-ethanoanthracene-11,12-dihydrazide) and are represented in table 2. The data of metal complexes revealed three possible tautomeric forms for the thiosemicarbazide; Keto/ thione, enol-thione and keto/thiol forms.

The IR spectrum (fig.1a) of the free TSc (Structure 1) shows three bands in the region 3371–3060 cm^{-1} attributable to stretching modes of the (N^4H), (N^2H), $\nu(N^1H)$ and aromatic CH vibrations, respectively. In the ir spectra of metal complexes, these bands appeared broad arising from the overlap of the stretching vibrations of lattice water molecules with the ν(NH)'s [26].The bands due to carbonyl group are observed as doublet at 1710 and 1680 cm^{-1} due to ν(CO) (free) and hydrogen bonded ν(CO) modes which is confirmed by the band at 3415 cm^{-1} [27].The appearance of $\nu(N^1H)$ at lower wavenumber in addition to weak bands at 1900-2100 and 2300-2500 cm^{-1} regions confirm the presence of intramolecular hydrogen bonding N-H-O [27].

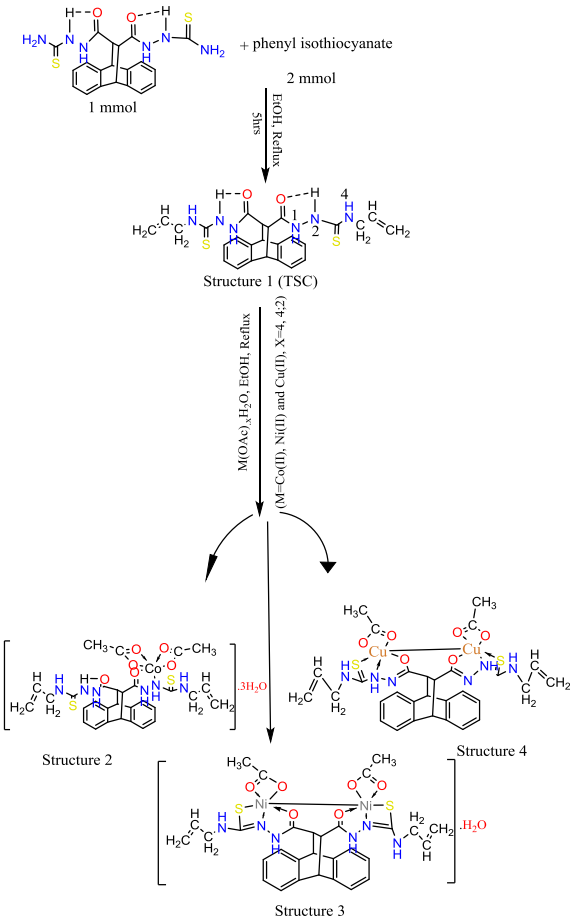

Scheme 1

The medium bands located at 1518, 1291, 917 and 790 cm^{-1} in the spectrum of the thiosemicarbazide may be assigned to thioamides I-IV that have substantial contributions from ν(C=N), δ(C-H) and δ(N-H) [28]. The band due to ν(N-N) is observed at 1050 cm^{-1}. Also, the doublets at 2931 and 2971 cm^{-1} are attributed to symmetric and asymmetric stretching vibrations of -CH_2- and CH groups while that due to $\nu(C=C)_{phenyl}$ appeared at 1596 cm-1. The possibility of thione /thiol tautomerism in the solid state is ruled out, since no characteristic bands for thiol group (2500-2650 cm^{-1}) are observed in the spectrum of the ligand [27].

An insight at the ir spectrum (fig.1b) of mononuclear [Co(TSC)$(OAc)_2$].3H_2O complex (Structure 2) reveals that the ligand behaves as neutral NO bidentate in keto-thione form through carbonyl

oxygen and N^2H nitrogen forming a five membered chelate ring. This mode of coordination is supported by disappearance of the bands at 1680 and 3289cm^{-1} assignable to $\nu(C=O)_{free}$ and $\nu(N^1H)$ in the ligand spectrum to lower wavenumber [28]. The band due to $\nu(C=O)_{bonded}$ remains unaltered confirming the mononuclear nature of the complex. The TSC coordinates in keto-thiol form in the binuclear $[Ni_2(TSC\text{-}2H)(OAc)_2].H_2O$ (Structure 3) as $N_2S_2O_2$ hexadentate binding two metal ions through two C-S formed, two C=O and two new (C=N*) groups (fig.1c). The later new azomethine group is formed as a result of conversion of two C=S→2C-SH followed by loss of two protons upon coordination. This mode is supported by disappearance of bands due to $\nu(N^2H)$ and ν/δ (C=S) with simultaneous appearance of new bands at 1585 and 635 cm^{-1} assigned to new ν (C=N*) and ν (C-S) respectively.Finally, in the binuclear complex, $[Cu_2(TSC\text{-}2H)(OAc)_2]$(Structure 4), TSC binds to metal ion in enol-thione form via O atoms of two C-O, N of two N^2H and S of two C=S groups coordinating two metal ions in a five membered rings. This postulation is confirmed as no bands due to (C=O) (at 1710 & 1680 Cm^{-1}) were observed, whereas new bands attributed to new ν (C=N*) and ν (C-O) modes appeared at 1567 and 1151 cm^{-1}, suggesting enolization of C=O groups with loss of two protons from the latter groups on coordinating the metal ions. The shift the band due to ν(C=S), and weakness of that due to ν (N^2H) confirms contribution in coordination [28].Also, the shift of ν(N-N) to higher wavenumber as a result of contribution of azomethine group in coordination[28].

The new bands at 509-528 and 422-469 cm^{-1} in the IR spectra of all complexes, the appearance of new bands at 509-528 and 422-469 cm^{-1} attributable to ν (M-O) [28] and ν (M-N) [27], respectively. The coordination of the acetate group in the title complexes is confirmed by the broad bands at at {(1532, 1437); (1454, 1346) and (505, 1419)} cm^{-1} characteristic for $\nu_{asy}(OCO)$ and $\nu_{sy}(OCO)$ affording wavenumber difference separation values ($\Delta\upsilon$=105, 108 &98 cm^{-1}), respectively lying in the range reported for bidentate acetate group [29].

Moreover, the presence of water in the hydrated complexes is supported by the existence of bands in the 3440-3400, 1640—1610 and 960-955 cm-1 ranges are due to $\nu(OH)_{stretching}$, $\nu(HOH)_{deformation}$ and $\nu(H_2O)_{rocking}$ vibrational modes. On the other hand, the band at 3500 cm-1is due to coordinated water. This notification will be supported by thermal analysis [29].

3.2. NMR spectra

The ^1H NMR spectrum of TSC in d6-DMSO (Fig. 2a) shows signals at δ= 9.23, 9.16 and 7.72 ppm referring to the N1H, N^2H and N^4H protons. These signals disappear upon addition of D_2O, which suggests that they are easily exchangeable. These protons are shifted downfield because they are easily subjected to hydrogen bonding with CO or CS that is confirmed by a signal at 10.05 ppm. The protons of each N^4H appeared as a singlet as expected since the NH protons are decoupled from the nitrogen atoms and the protons from the adjacent atoms. But contrary to this, N^1H and N^2H protons show coupling with the adjacent hydrogen and hence gives a doublet. This coupling can be attributed to the low NH exchange rate. The multiplets at δ = 6.98-7.31 ppm are assigned to the protons of phenyl groups [30]. The protons of CH groups (CH13-CH14) (Structure 47 a) appear at 3.34, 3.22(dd, J=3.6, 1H) and (CH15-CH19) as multiples at 3.42-3.50 ppm. The two quartet signals observed at 3.99-4.20 and 5.03-5.12 ppm and the two doublets at 3.07-3.63 and 3.70-4.12 and 4.27 ppm are assignable to the protons of $CH_2(-N^4H-CH_2)$ and $CH_2(CH=CH_2)$ groups, respectively. Moreover, the sexet signal centered at 5.80 ppm is assigned to the protons of the allyl CH group. According, it may be suggested that the thiosemicarbzide, TSC can exist in more than one form arising with different orientations with respect to the $-CH_2-CH=CH_2$ groups. Finally, the absence of SH signal confirmed the presence of the ligand in the thione-keto-enol form in the solution [20].

The ^{13}C NMR spectrum (fig.2b) indicated the presence of 26 carbon atoms in TSC including four aliphatic methine groups at δc 45.2 and 46.6 ppm, two methylene groups at 45.9, two amidic carbon atoms at 171.6, two thione groups at 181.8 and 12 aromatic carbon atoms from 115.6 to 142.9 ppm including, two olefinic carbon atoms at 115.6 and 134.8 ppm for CH_2-30 and CH-29, respectively [31].

3.3. Electronic spectra and magnetic moments

Table 3 shows the data obtained from electronic absorption bands of TSC and its divalent metal complexes displayed in DMSO. The spectrum of the TSC (fig.3a) exhibited two shows two broad bands at 33599 cm-1 (297.00nm); 36495 cm-1 (274.01nm) & 33785 (295.98nm), presumably arising from π→π* and n→π*, a combination of the transitions due to those of benzene ring, carbonyl and thione groups, respectively [32]. On comparing the spectra of the complexes with that of the TSC, the following important notifications can be drawn:

i. The spectra of metal complexes showed intra-ligand bands at 35971-36101 and 33599-32051 cm^{-1} attributed to π→π* transition of phenyl ring and carbonyl and/or thione groups, respectively. The n→π* transition bands suffer a noticeable great change upon complexation and appeared at 25188-27397 cm^{-1} indicating the chelation of central metal ion through the carbonyl and thione groups.

ii.The electronic spectrum of $[Co(TSC)(OAc)_2].3H_2O$

complex (fig.3b) exhibits two bands at 14859 and 23259 cm^{-1} assignable to $^4T_{1g}(F) \rightarrow {}^4A_{2g}(F)$ (υ2) and $^4T_{1g}(F) \rightarrow {}^4T_{1g}(P)$ (υ3) transitions, respectively, in an octahedral configuration [33]. The calculated values of Dq, B and β (963.5, 849 &0.87) lie in the range reported for octahedral Co (II) complexes. Also, the band at 24390 cm^{-1} would be assigned to L-Co(II) CT caused by π bond resulting from bonding orbital formed by d_{x2-y2} orbital of the central metal and 3p orbital of the ligand donor atom. Moreover, the CT band of 25575 $cm^{-1}$is assigned by σ bond resulting from the same bonding orbital. The magnetic moment value per one Co (3.12 B.M.) is low due to strong M-M interaction and consistent with that of mixed phosphine arsine complexes [33].

iii.The broad in $[Ni_2(TSC\text{-}2H)(OAc)_2].H_2O$ complex (fig.3c) shows two bands at 15635 and 25316 cm^{-1} assignable to $^3A_{2g}(F) \rightarrow {}^3T_{1g}(F)$ and $^3A_{2g}(F) \rightarrow {}^3T_{1g}(P)$ transitions, respectively in an octahedral environment. The values of the ligand field parameters Dq, B, and β (978.5, 772 & 0.74), as well as the magnetic moment value (2.61 B.M.), are consistent with Ni(II) octahedral geometry [33] as well as the magnetic moment value per one metal atom ($\mu_{eff.}$ =1.198 B.M.) which is very low compared to that of the free electron (1.73 B.M.) that is an evident of strong M-M interaction.

iv.The bands at 12469 and 20408 cm^{-1} assignable to $^2B_{1g} \rightarrow {}^2E_g$ and $^2B_{1g} \rightarrow {}^2A_{1g}$ transitions in the spectrum of the complex, $[Cu_2(TSC\text{-}2H)\ (OAc)_2]$ complex (fig.3d) supports an octahedral geometry. The band at 21231 cm^{-1} is referred to S→Cu transition [34]. In addition, higher energy band intense bands at 23753 and 28571 cm^{-1} may be due to O→ Cu and N→ Cu charge transfer transitions Also, the magnetic moment value per one metal atom ($\mu_{eff.}$ =1.23 B.M.) is subnormal and lower that for one free electron (1.73 B.M.) revealing strong Cu-Cu interaction which will be supported by ESR spectrum [34].

3.4. Electron spin resonance

The solid stateroom temperature X-band ESR spectrum of [Cu2(TSC-2H) (OAc)2] complex is illustrated in figure 4. The spectrum visualizes a strong and wide signal with hyperfine splitting (giso = 2.04) suggesting that present TSC (ONS) chelating system seems to be coplanar with the two five-membered chelate rings adopting the nearly planar octahedral structure ($g_{\parallel}$ (2.08) > $g_{\perp}$(2.109). The interaction between the two Cu(II) ions that expressed by G =1.96 which is < 4.0 that indicates an appreciable interaction between metal ions in the solid that is supported by the subnormal magnetic moment value ($\mu_{eff.}$ =1.23 B.M) and in agreement with the binuclear nature of the investigated Cu(II) solid complex. Also, the hyperfine splitting for parallel orientation value ($A_{\parallel}$ =0.0006) is larger than those for the perpendicular one (A⊥= 0.0072) revealing that the singled electron is in a - nonbonding orbital away from the equatorial plane ligands and this is consistent with the literature. The molecular orbital coefficient (α^2) for in-plane σ bonding and β^2 (π bonding) were calculated according to the equations:

$\alpha^2 = (A_{\parallel}/ 0.036) + (g_{\parallel} - 2.0023) + 3/7\ (g_{\perp} - 2.0023) + 0.04$

$\beta^2 = (g_{\parallel} - 2.0023)\ E/8\lambda\alpha^2$

Where λ = -828 cm^{-1} for the free copper ion and E is the electronic transition energy. The α^2 (measure of the covalency of the in-plane σ bonding) is found to be 0.39 and the β^2 parameter (measure of the covalency of the in-plane π bonding) is 0.51 indicating that the in-plane σ-bonding is more covalent and in good agreement with previous work [35].

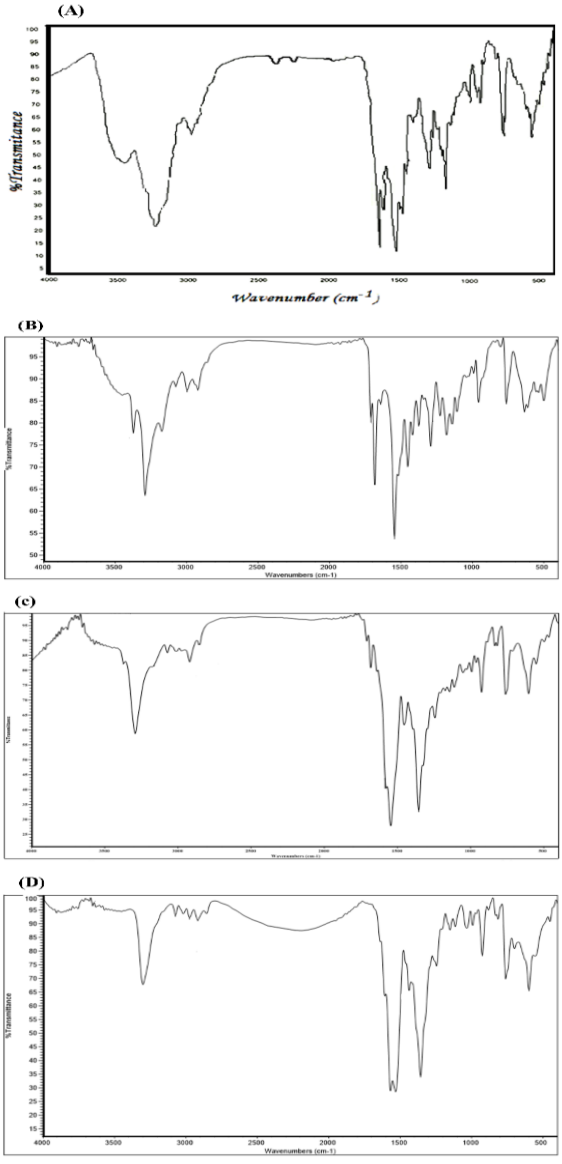

Figure (1) IR spectral bands (KBr discs). TSC ligand (A), $[Co(TSC)\ (OAc)_2].3H_2O$ complex (B),$[Ni_2(TSC\text{-}2H\ )(OAc)_2].2H_2O$ complex(C), $[Cu_2(TSC\text{-}2H)(OAc)_2]$ complex (D).

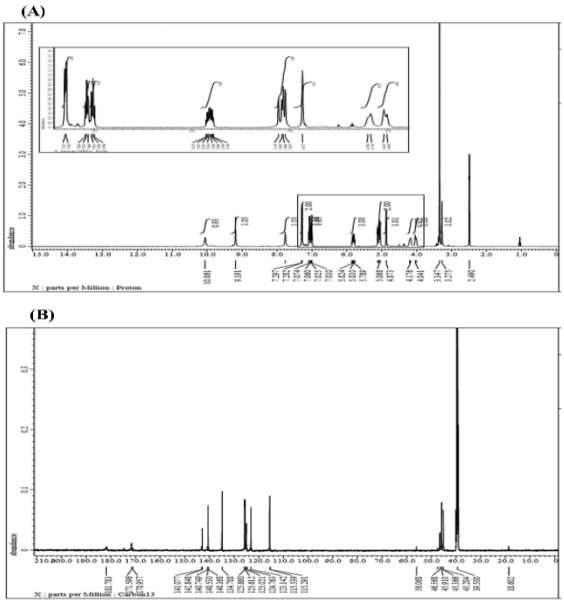

Figure 2: NMR spectra of TSC in d_6DEMSO. ^{1}HNMR(A), ^{13}CNMR (B).

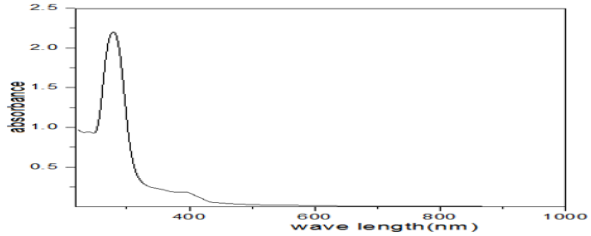

(A)

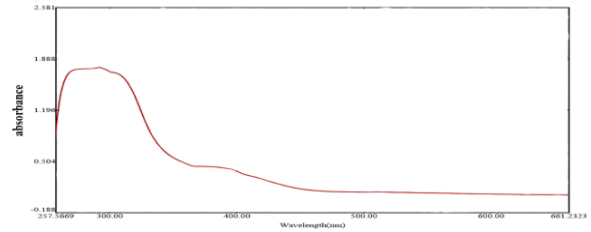

(B)

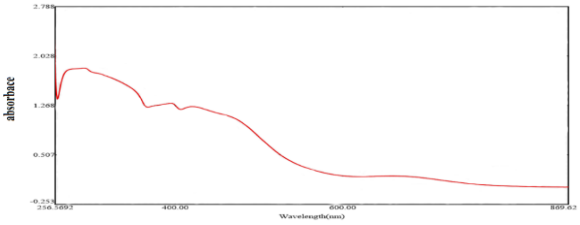

(c)

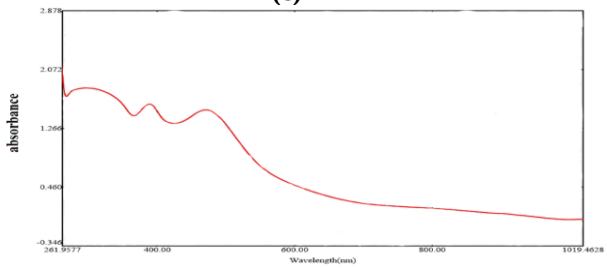

(D)

Figure 3. UV-vis. Spectra in DMSO TSC ligand (A), $[Co(TSC)(OAc)_2].3H_2O$ complex (B), $[Ni_2(TSC\text{-}2H)(OAc)_2].2H_2O$ complex (C), $[Cu_2(TSC\text{-}2H)(OAc)_2]$ complex (D).

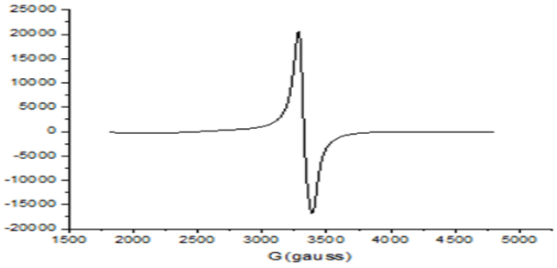

Figure 4.X-band ESR spectrum of $[Cu_2(TSC\text{-}2H)(OAc)_2]$ complex.

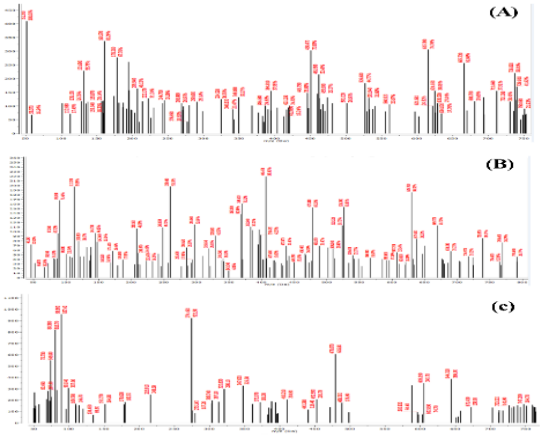

Figure 5. Mass spectra of metal complexes.$[Co(TSC)(OAc)_2].3H_2O$ complex(A),$[Ni_2(TSC\text{-}2H)(OAc)_2].2H_2O$ complex (B),$[Cu_2(TSC\text{-}2H)(OAc)_2]$ complex (C).

Mass spectra

The mass spectra of all complexes and the molecular ion peaks that confirms the suggested molecular formulae are recorded in Table 1 and graphically in figure 5. As a typical example, the mass spectrum of $[Ni_2(TSC\text{-}2H)(OAc)_2].H_2O$ (Fig. 5b) which showed peaks that corresponding to the successive degradation of the metal complex. The appearance of a molecular ion peak at m/ e =791.64 (Rel.Int: %39.74) is in agreement with the molecular mass (791.65). The second peak at m/e = 774.21 is corresponding to the removal of one lattice H_2O molecule after which multi peaks are observed. The peak at m/e = 629.70 (Calcd. 630.00 & Rel.Int: % 84.50) represents the $C_{26}H_{22}N_6Ni_2O_2S_2$ fragment that corresponding to removal of 2OAc + H_2O +4H fragments while that at 406.47(Rel.Int:% 100) corresponds to $C_{20}H_{18}Ni_2O_2$ fragment and that at m/e = 144.75 (Rel.Int.:44.01) is corresponding to $C_3H_2NiO_2$ fragment. The base peak at m/ e = 58.05 represents Ni isotope.

Table 1: Analytical and physical data of TSc` s and their divalent metal complexes

Compound	Empirical formula	F.wt. Found (Calcd)	Color	M.p. ◦c	Elemental analyses % Found (Calcd)				
					C	H	N	S	M
(1)	TSC $C_{28}H_{32}N_4O_2S_2$	520.00* (520.67)	white	265	59.84 (59.97	5.49 (5.42	15.94 (16.14	12.10 (12.31	-
(2)	[Co(TSC)(OAc)$_2$].3H$_2$O	750.680* (751.738	Brownish green	>300	50.94 (51.65	5.21 (4.41	11.89 (12.05	9.54 (9.19)	9.01 (8.45)
(3)	[Ni$_2$(TSC-2H)(OAc)$_2$].2H$_2$	790.336* (791.650	Dark brown	>300	45.90 (46.67	5.01 (4.44	15.20 (14.86	8.30 (8.46)	15.79 (14.86
(4)	[Cu$_2$(TSC-2H)(OAc)$_2$]	(763.83)	Pale green	>300	48.11 (47.17	4.58 (4.22	10.67 (11.00	8.39 (9.17)	16.88 (16.64

*obtained by mass spectra

Table 2: Assignment IR bands of TSC and its divalent metal complexes

Compound	ν(N^4H)	ν(N^2H)	ν(N^1H)	ν(N-N)	ν(C=O)	ν/ δ C=S)	ν (C=C)	ν(C=N*)	ν (C-O)
(1)	3375_m	3171_m	3281_s	1021	1710_m 1680_s	1290_s 799_s	1610_m	-	-
(2)	3281_m	31731_w	3290_w	1043_m	1710_m 1671_w	1291_s 793_s	1596m	-	1180_m
(3)	3371_s	3189s	3292_w	1023_m	1710_m 1680s	-	1597_m	1585_m	-
(4)	3301_m	3185_{vw}	3301_m	1033_b	-	1290_w 762_w	1595_m	1567_m	1151_m

Table 3. Spectral absorption bands, magnetic moments and ligand field parameters of ligands and their divalent complexes.

Compound	Band position, nm	Band position, cm^{-1}	μ_{eff} (B.M.)	Ligand field parameters			Geometry
				D_q (cm^{-1})	B (cm^{-1})	β	
TSC(1)	297, 356	33500, 28090	--	--	--	--	--
(2)	292,307 391, 410 430, 905	34246, 32573 25575, 24390 23255, 11049	3.120	963.5	849	0.87	Oct.
(3)	291, 395 420, 673	34364, 25316 23809, 14859	1.198*	978.5	772	0.74	Oct.
(4)	296, 389 471, 490 802	33783, 25707 21231, 20408 12469	1.230*	-	-	-	Oct.

*: per one atom.

3.6. Thermal study

The TG curves of the complexes are represented in figure 6 and the decomposition steps with released species as well as the weight loss are listed in table 4. TG (Thermogram) of TSC derivative and its metal complexes displayed 3, 4, 3 and 4 decomposition stages, respectively. TG of [Co (TSC)(OAc)$_2$].3H$_2$O as an example (fig.6a), indicates that the first degradation step (36-117 ^{o}C) with weight loss (Found:4.57% (Calcd.4.57%) is due to loss of two lattice water molecules. The second step with weight loss (found:33.16%; Calcd. 32.49%) at 118-234^{o}C is attributed to the elimination of $H_2O+2H_2S+2OAc+2N_2$.The third step (235-287^{o}C) with weight loss (found:12.87%; Calcd. 13.58%) is referring to the removal of $2C_3H_5N$ fragments. The fourth step with weight loss (found:19.15%; Calcd. 19.66%) at 288-350 ^{0}C is due to removal of $2C_6H_4$+3H fragments. The residual part is metal oxide and C/or S.

3.7. Thermodynamic and kinetic studies

Coats-Redfern [36] and Horowitz-Metzger [37] methods were used to estimate kinetic parameters of the title compounds and the data are represented graphically in figure 7 and 8 and table 5. It is obvious that ΔS*(entropy of activation) is negative indicating that the activated fragments are more ordered than the un-decomposed ones, the values ΔH* (enthalpy of activation) are positive indicating an endothermic

nature of decomposition processes. The high values of E_a reveal the high stability of such chelate due to their covalent bond character. Also, the positive sign of ΔG* reveals that all decomposition steps are nonspontaneous and increasing regularly which may be referred to the structural rigidity of the remaining complex after the expulsion of one or more ligands [38].

3.8.DFT Study

DFT method is one that conveys the chemical reactivity as well as the site selectivity of molecular systems. The energies of the frontier molecular orbitals (E_{HOMO}, E_{LUMO}) (figs.9-12 C & D), the energy band gap which explains the eventual charge transfer interaction within the molecule, electronegativity (v), chemical potential (l), global hardness (g), global softness (S) and global electrophilicity index (x) [39] are evaluated according to literature [40] and the data recorded in Table 6. This new reactivity index measures the stabilization in energy when the system acquires an additional electronic charge from the environment. The importance of g and r is in measuring the molecular stability and reactivity. The concepts of the parameters v and the chemical potential l are related to each other. From the obtained data we can deduced that: 1. Absolute hardness g and softness r are important properties to measure the molecular stability and reactivity. A hard molecule has a large energy gap and a soft molecule has a small energy gap. Soft molecules are more reactive than hard ones because they can easily offer electrons to an acceptor. In a complex formation system, the ligand acts as a Lewis base while the metal ion acts as a Lewis acid. Metal ions are soft acids and thus soft base ligands are most effective for complex formation. Accordingly, it is concluded that ligands, with a proper r value have a good tendency to chelate metal ions effectively [41, 42]. This is also confirmed from the calculated chemical potential l. 2. This reactivity index measures the stabilization in energy when the system acquires an additional electronic charge (DN_{max}) from the environment. The electrophilicity index (v) is a positive, definite quantity and the direction of the charge transfer is completely determined by the electronic chemical potential l of the molecule because an electrophile is a chemical species capable of accepting electrons from the environment and its energy must decrease upon accepting electronic charge. Therefore, the electronic chemical potential must be negative, exactly as supported by the values in Table 6.

3.8.1. Molecular electrostatic potential (MEP)

The MEP is a plot of the electrostatic potential mapped onto the constant electron density surface. It is also very useful for the research of molecular structures with its physiochemical property relationship as well as for hydrogen bonding interactions [42]. The electrostatic potential V(r) at a given point r (x, y, z) is defined in terms of the interaction energy between the electrical charge generated from the molecule's electrons, nuclei and proton located at r. Computation of the electrostatic potential is possible for molecules using the C-point and multiple k-points. In the present study, 3D plots of the molecular electrostatic potential (MEP) of the ligands (Figs. 9-12B) have been drawn. The maximum negative region, which is the preferred site for electrophilic attack, is indicated in red, the maximum positive region, which is the preferred site for nucleophilic attack, in given in bluer. The potential increases in the order red < green < blue, where blue shows the strongest attraction and red shows the strongest repulsion. Regions having the negative potential are over the electronegative atoms while the regions having the positive potential are over the hydrogen atoms.

3.8.2. Geometry optimization

From the data listed in Tables 8 and 9 that contain the bond lengths and bond angles, one can withdraw the following important remarks:

i. An elongation is observed in the coordination bonds upon complexation which results in lowering of energy for the bond's vibration and in turn lowering the frequency of vibration and is in accord with the experimental IR frequency values.

ii. For TSC ligand, the bond lengths; C(16)–O(23), C(20)–O(34), N(27)–C(28), C(26)-N(27), C(24)-N(25), C(24)- S(35), C(26)- S(36), C(20)-N(21), N(21)-N(22) and N(17)-N(18) become slightly longer in the complex as coordination takes place *via* N(18) of N^2H group, along with the O(23) and O(34) atoms of C=O groups.

iii. C(16)–O(23) and C(20)–O(34) and C(20)–O(34) bond distances in all complex becomes longer due to the formation of the M–O bond, which makes the C–O bond weaker [43].

iv. Also, for TSC, the C(24)- S(35), C(26)- S(36), C(26)- S(36), H(53)–N(25) and H(54)–N(22) bond lengths become slightly longer especially in the binuclear Ni^{2+} and Cu^{2+} complexes as the coordination takes place via the S atoms of two C=S groups. The C(12)–S(17) group enolized leading to the absence of double bond character over C(12)–S(17) and its appearance over N(11)–C(12). The C(16)–O(23) and C(20)–O(34) are enolized leading to the absence of double bond character over either C(16)–O(23) or C(20)–O(34) and its appearance over N(17)– C(16) and N(21)-C(26) bond distance in the Cu^{2+} complex becomes longer due to the formation of the M–O bond which makes the C–O bond weaker.

v. The bond angles of the thiosemicarbazide moiety, TSC are altered somewhat on coordination; the largest changes affect the C(26)–N(22)–N(21), N(25)-C(24)-N(18), S(35)-C(24)-N(25), S(35)-C(24)-N(18), O(34)–C(20)–N(21), O(34)–C(20)–C(19), H(51)-N(21)-C(20), N(22)-N(21)-C(20), O(23)–C(16)–N(17), O(23)–C(16)–C(15), N(18)–N(17)-C(16), S(36)–C(26)-N(27) and S(36)–C(26)-N(23) [44].

3.9. Biological activity

3.9.1.DNA binding

In this assay the DNA value (the difference between DNA/methyl green complex and free cabinol) provides the simplest means for detecting the DNA-binding affinity and relative binding strength. The results were reported as a 50% inhibition concentration value (IC_{50}) calculated by linear regression of data plotted on a semi-log scale and recorded in Table 10. Doxorubicin was used as positive control [45]. The data revealed a potent good inhibitory activity displayed by the thiosemicarbazide ligand, TSC (IC_{50}; %35.26 ± 2.2) that is similar to the standard (DOX; IC50; %31.26± 1.5) meaning. This means it potently intercalate DNA. On the other hand, Co (II) complex exhibited an inhibition activity of (IC50; %57.26 ±2.6); Cu (II) complex (IC50; %81.95 ±6.2) and Ni (II) complex (IC50; %89.25 ±3.2), respectively.

According to the obtained results, we could deduce valuable data about the structure activity relationships. In case of free TSC, the availability of numerous active sites such as six secondary NH, two C=O, two thione groups as well as the planarity of the phenyl rings that can intercalates toward the minor groove the Cyt5 and Gua6 and the sugar moiety formed hydrogen bonds with nitrogen bases such as Cyt5 and Gua6 [41]. Also, the same in case of the mononuclear Co (II) complex, there are still three NH, one C=O and one thione groups free. In contrast to the other binuclear Ni (II) and Cu (II) complexes, most of active sited are bounded to the two metal nuclei.

3.9.2.SOD activity

Table 11 shows the data obtained from SOD-like activity assay. The observed values of superoxide scavenging activity are comparable and even better placed compared to that of the various well established [5]. It may be concluded that TSC (potent activity;(%77.85), Co-complex (% 67.00) and Ni-complex (%62.30) are good SOD mimic scavengers comparable to the standard drug, ascorbic acid (%78.20). The difference in the nature of the chelating ligand and/or the extent of distortions in the overall geometry is usually responsible for the observed variations in their SOD activities. TSC has all active sites free for can donate hydrogen atoms or an electron thus contribute to increase the antioxidant activity and also, Co- complex exhibits higher activity followed by Ni- complex higher activity than Cu- complex. This is in accordance with the fact that the complexes with small molecular weight displays better activities than that experienced by the large or polymeric compounds [46].

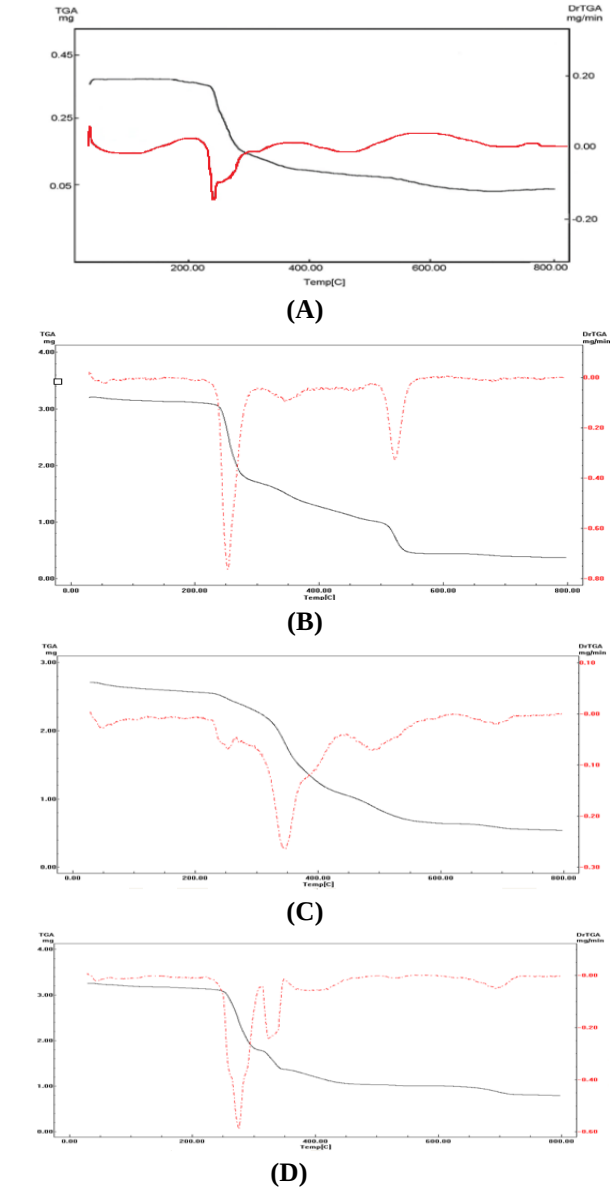

Figure 6. TGA curves. TSC (A),[Co(TSC)$(OAc)_2$].$3H_2O$ complex(B), [Ni_2(TSC-2H)$(OAc)_2$].$2H_2O$ complex (C),[Cu_2(TSC-2H)$(OAc)_2$] complex (D).

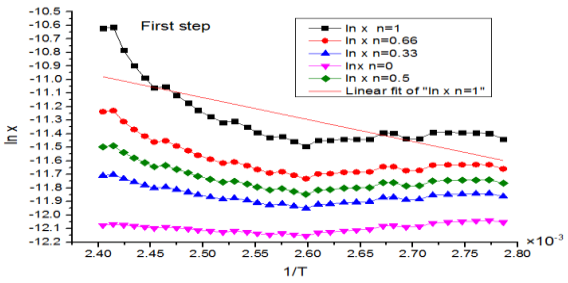

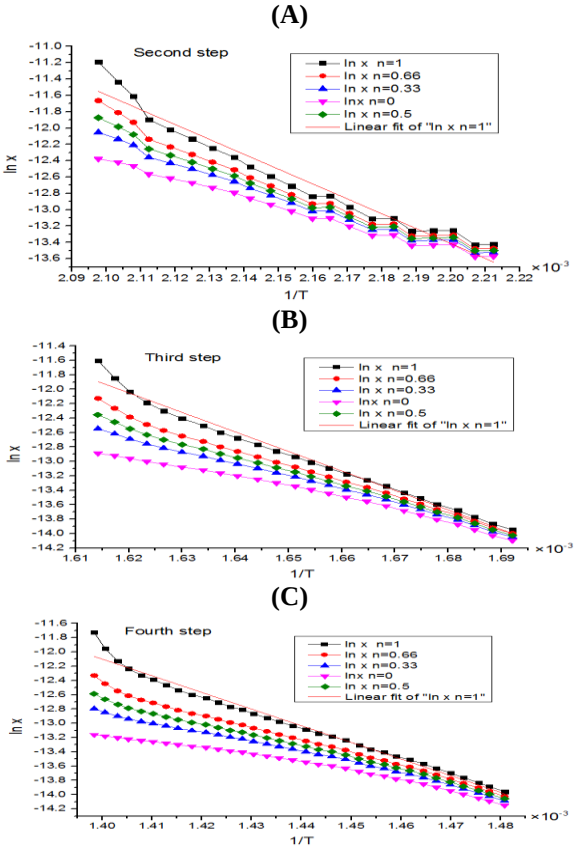

Figure 7. Coats-Redfern plots of [Co(TSC)$(OAc)_2$].3H_2O.first degradation step (A),second degradation step (B), third degradation step (C), fourth degradation step (D).

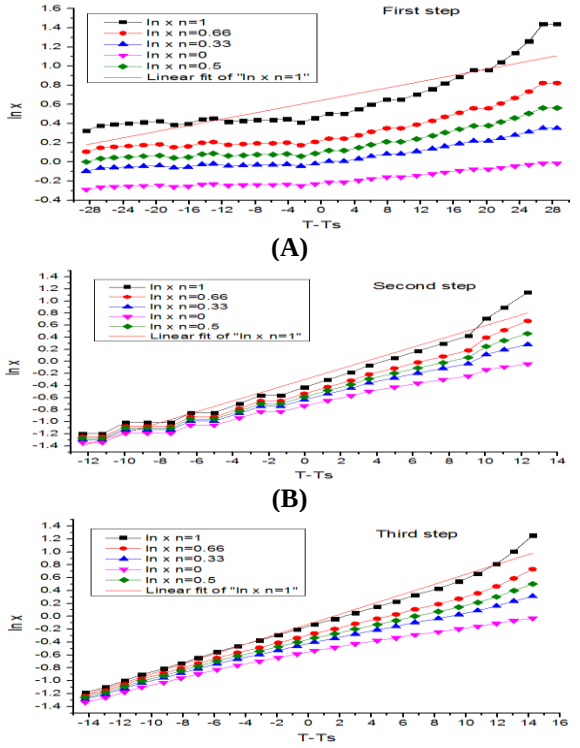

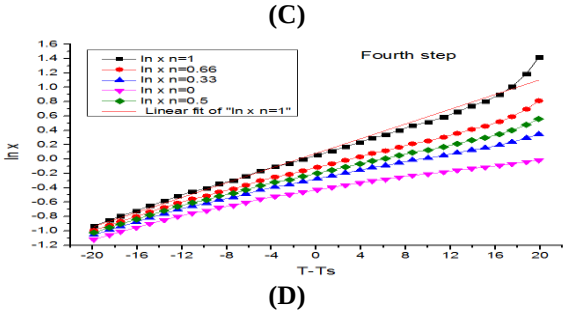

Figure 8. .Horowitz-Metzger plots of [Co(TSC)$(OAc)_2$].3H_2O. first degradation step (A), second degradation step (B), third degradation step (C), fourth degradation step (D).

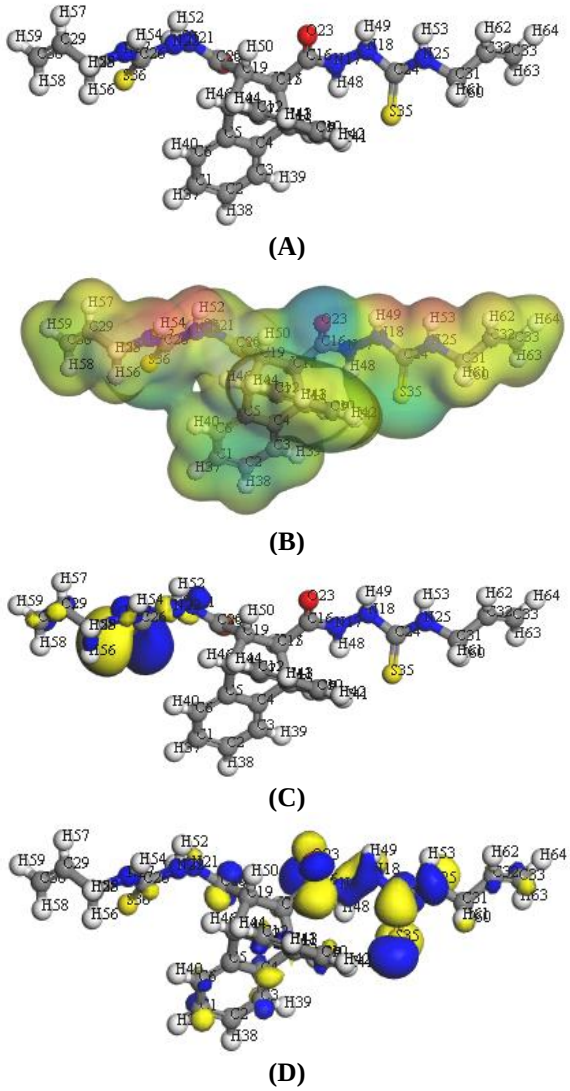

Figure 9. Molecular modeling of TSC. Geometry optimization (A), MEP (B), HOMO(C), LUMO (D).

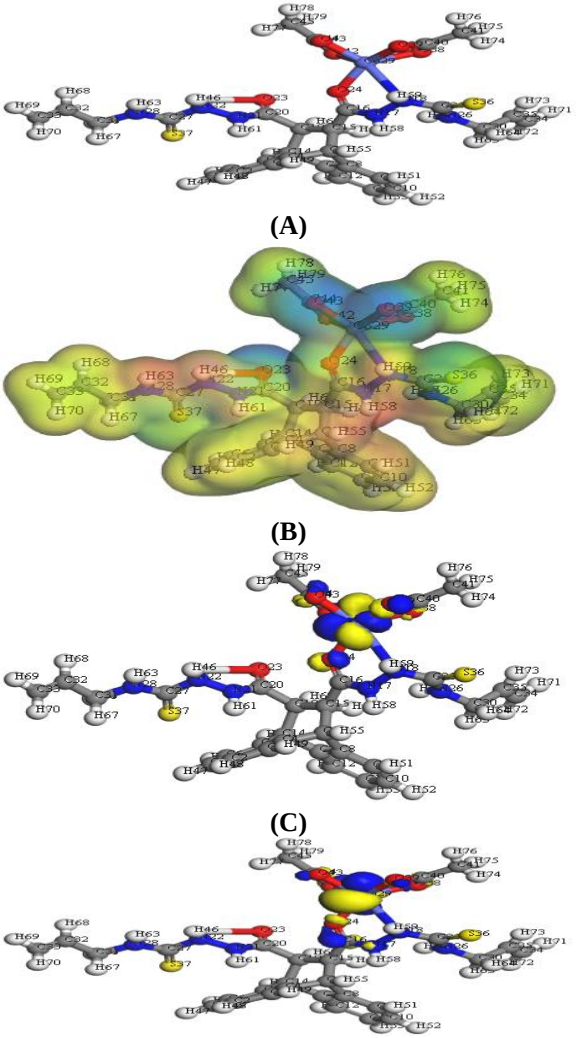

Figure 10. olecular modeling of [Co(TSC)$(OAc)_2$].3H_2O. Geometry optimization (A), MEP (B), HOMO(C), LUMO (D).

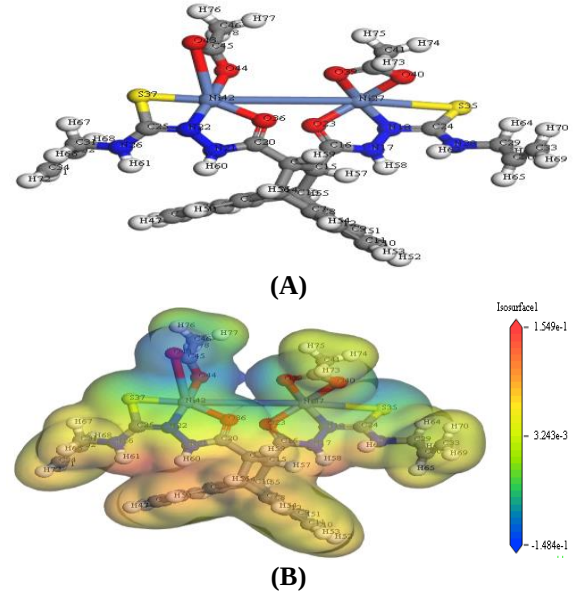

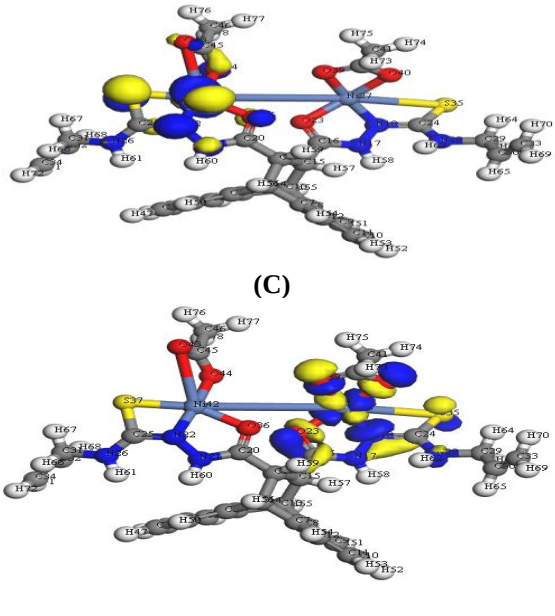

Figure 11. Molecular modeling of [Ni_2(TSC-2H)$(OAc)_2$].2H_2O. Geometry optimization (A), MEP (B), HOMO(C), LUMO (D)

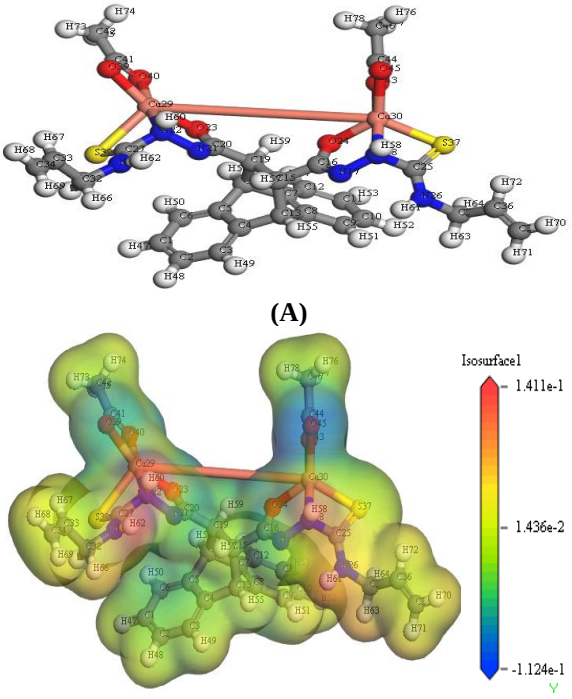

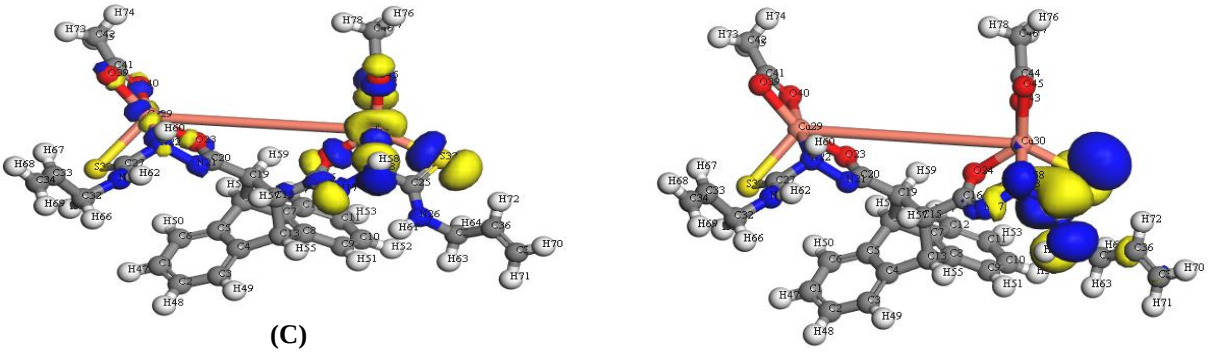

(C) **(D)**

Figure 12. Molecular modeling of $[Cu_2(TSC-2H)(OAc)_2]$. Geometry optimization (A), MEP (B), HOMO(C), LUMO (D).

Table 4: Decomposition steps with the temperature range and weight loss for TSC and its divalent metal complexes

Compound	Step	Temp. rang (°C)	Removed species	Wt. loss %	
				Found	Calcd
TSC	1st	223-290	$N_2+2C_6H_4+2H_2S+2H_2O$	56.48	55.39
	2nd	291-379	$-C_6H_{10}$	14.22	15.78
	3rd	480-649	$-N_2+N_2H_2$	9.79	10.75
	Residue	650-800	8C	19.00	18.45
$[Co(TSC)(OAc)_2].3H_2O$	1st	36-117	$-2H_2O$	4.20	4.57
	2nd	118-234	$-H_2O+2H_2S+2OAc+2N_2$	33.16	32.49
	3rd	235-287	$-2C_3H_5N$	12.87	13.58
	4rd	288-350	-2C6H4+3H	19.15	19.66
	Residue	351-800	2CoO+7C	30.62	29.70
$[Ni_2(TSC-2H)(OAc)_2].2H_2O$	1st	29-101	$-H_2O$	3.11	2.33
	2nd	102-443	$-6NH_3+C_{26}H_{14}O$	57.78	57.58
	3rd	444-621	$-C_4O+SO_2$	15.81	16.59
	Residue	622-800	2NiO+S	23.30	23.50
$[Cu_2(TSC-2H)(OAc)_2]$	1st	29-139	$-NH_3$	2.43	2.23
	2nd	140-310	$-5NH_3+C_{19}H_{14}$	42.84	42.87
	3rd	311-350	$-C_6O_2$	12.90	13.62
	4rd	351-640	$-C_5O_2$	11.78	12.05
	Residue	641-800	2CuO+2S	30.05	29.23

Table 5. Kinetic parameters evaluated by Coats-Redfern and Horowitz equations for and TSc`s and their divalent (II) complexes

	peak	Mid Temp(K)	Ea KJ\mol	A (S^{-1})	ΔH* KJ\mol	ΔS* KJ\mol.K	ΔG* KJ\mol
(1)	1st	512.07	168.44	$1.92\times10^{+12}$	164.19	-0.01423	171.48
		520.4	*158.77*	*1.65×10^{14}*	*154.44*	*-0.0226*	*142.67*
	2nd	625.61	106.17	$1.06\times10^{+4}$	100.97	-0.02093	209.85
		624.17	*116.73*	*88311674.33*	*111.54*	*-0.0989*	*173.30*
	3rd	840.87	204.21	$4.56\times10^{+7}$	197.21	-0.1069	287.11
		840.43	*218.22*	*3.59×10^{11}*	*211.23*	*-0.03230*	*238.39*
(2)	1st	387.41	13.45	3.37E-01	10.23	-0.2561	109.45
		387.41	*20.35*	*4.31E+00*	*17.13*	*-0.2350*	*108.15*
	2nd	464.35	151.45	1.73E+15	147.59	0.0431	127.57
		464.35	*159.67*	*1.52E+16*	*155.81*	*0.0612*	*127.41*
	3rd	605.25	224.99	4.33E+17	219.95	0.0868	167.40
		605.25	*235.34*	*3.51E+18*	*230.31*	*0.1042*	*167.23*
	4th	695.20	194.04	5.02E+12	188.26	-0.0088	194.38
		695.20	*205.89*	*4.10E+13*	*200.11*	*0.0087*	*194.10*
(3)	1st	338.85	51.49	1.48E+06	48.67	-0.1279	91.99
		338.85	*57.22*	*1.24E+07*	*54.40*	*-0.1102*	*91.75*
	2nd	657.46	64.50	1.93E+06	59.03	-0.1312	145.28
		409.35	*71.68*	*1.73E+07*	*68.27*	*-0.1090*	*112.88*
	3rd	747.90	335.06	4.53E+21	328.84	0.1620	207.67
		747.90	*347.95*	*3.71E+22*	*341.73*	*0.1795*	*207.48*
(5)	1st	384.69	29.63	1.38E+02	26.43	-0.2061	105.70
		384.69	*36.18*	*1.29E+03*	*32.99*	*-0.1875*	*105.12*
	2nd	454.74	111.32	9.61E+10	107.54	-0.0382	124.90
		454.95	*119.12*	*7.97E+11*	*115.33*	*-0.0206*	*124.70*
	3rd	610.50	340.25	5.52E+27	335.18	0.2802	164.11
		610.50	*350.59*	*4.32E+28*	*345.51*	*0.2973*	*164.00*
	4th	664.65	205.74	2.22E+14	200.22	0.0230	184.90
		664.65	*217.06*	*1.80E+15*	*211.54*	*0.0405*	*184.65*

Table 6. Calculated E_{HOMO}, E_{LUMO}, energy band gap ($E_H - E_L$), chemical potential (μ), electronegativity (χ), global hardness (η), global softness (S), global electrophilicity index (ω) and softness (σ) for of TSc` s and its M(II) complexes

Compound	E_{HOMO}	E_{LUMO}	E_H-E_L	X	μ	η	S	ω	σ
TSC	-4.919	-1.32	-3.599	3.1195	-3.15	1.7995	0.2778	2.703	0.555
$[Co(TSC)(OAc)_2].3H_2O$	-4.233	-3.037	-1.841	-0.645	0.551	1.747	2.943	4.139	5.335
$[Ni_2(TSC\text{-}2H)(OAc)_2].2H_2O$	-4.145	-3.304	-2.463	-1.622	-0.781	0.06	0.901	1.742	2.583
$[Cu_2(TSC\text{-}2H)(OAc)_2]$	-4.461	-2.377	-0.293	1.791	3.875	5.959	8.043	10.127	12.211

Table 7. Selected DFT bond length (Å) of TSC ligand

Bond	TSC	Co^{2+} complex	Ni^{2+} complex	Cu^{2+}complex
C20-O34	1.269	1.266	1.219	1.226
C16-O23	1.067	1.184	1.223	1.273
C26-S36	1.617	1.627	2.075	1.551
N21 -N22	1.354	1.391	1.352	1.358
C26-N22	1.377	1.370	1.278	1.378
N 27-C28	1.465	1.378	1.476	1.464
N17-N18	1.352	1.341	1.350	1.359
C16-N17	1.366	1.342	1.363	1.271
C24-S35	1.581	1.582	1.874	1.429
C24-N18	1.375	1.410	1.275	1.702
C20-N21	1.399	1.512	1.371	1.263
C24-N25	1.377	1.381	1.264	1.357
N17 -H48	1.009	1.006	1.011	1.021
N18 -H49	1.014	1.019	0.601	0.603
N25 -H53	1.021	1.023	1.048	1.021
N21-H51	1.015	1.005	1.006	1.020
N22-H52	1.013	1.020	0.601	1.020
N27-H54	1.023	1.021	1.052	1.020
M-O	-	1.192	1.810, 1.79	1.819, 1.82
M-N	-	1.934	1.842, 1.839	1.951, 1.939
M-S	-	-	2.187, 2.179	2.160, 2.156
M1-O acetate	-	1.164, 1.235	1.826, 1.796	1.855, 1.817
M2-O acetate	-	1.210,1.168	1.793, 1.827	1.816, 1.853
M-M	-	-	2.323	2.363

Table 8. Selected DFT bond angles (^{0}) of TSC ligand and its M(II) complexes.

Bond angle	TSC	Co^{2+} complex	Ni^{2+} complex	Cu^{2+} omplex
C(32)-C(31)-N(25)	107.951	109.38	108.786	108.573
C(29)-C(28)-N(27)	108.56	108.585	114.613	109.410
C(28)-N(27)-C(26)	119.814	119.283	108.693	120.367
C(31)-N(25)-C(24)	123.827	124.216	108.786	121.451
N(27)-C(26)-N(22)	167.732	168.57	171.35	139.61
N(25)-C(24)-N(18)	113.658	114.034	131.515	113.976
C(26)-N(22)-N(21)	117.46	124.997	109.739	113.573
N(22)-N(21)-C(20)	114.995	100.897	113.795	113.17
N(21)-C(20)-C(19)	153.187	113.469	115.674	120.59
C(24)-N(18)-N(17)	124.129	104.636	107.819	107.76
N(18)-N(17)-C(16)	117.58	114.64	113.795	118.93
N(17)-C(16)-C(15)	115.70	113.41	116.624	117.26
S(36)-C(26)-N(27)	84.156	83.303	125.492	74.36
S(36)-C(26)-N(22)	83.584	85.296	72.844	74.30
S(35)-C(24)-N(25)	124.025	125.179	125.173	144.96
S(35)-C(24)-N(18)	122.277	120.787	103.253	146.06
O(34)-C(20)-N(21)	80.963	98.763	119.108	116.31
O(23)-C(16)-N(17)	120.994	127.205	117.678	116.06
O(34)-C(20)-C(19)	72.224	82.342	122.602	119.24
O(23)-C(16)-C(15)	123.256	152.568	126.036	122.57
H(61)-C(31)-N(25)	109.918	108.126	108.356	109.31
H(56)-C(28)-N(27)	109.812	111.297	111.651	109.92
H(54)-N(27)-C(26)	125.166	118.081	117.073	123.39

Table 9: DNA/methyl green colorimetric assay of the DNA-binding compounds.

No.	DNA-active compound	DNA/methyl green (IC_{50}, µg/ml)
	DOX	31.54±1.5
1	TSC	35.26 ± 2.2
2	$[Co(TSC)(OAc)_2].3H_2O$	57.26±2.6
3	$[Ni_2(TSC\text{-}2H)(OAc)_2].2H_2O$	89.25±3.2
4	$[Cu_2(TSC\text{-}2H)(OAc)_2]$	81.95±6.2

***IC_{50} values represent the concentration (mean ± SD, n = 3-5 separate determinations) required for a 50% decrease in the initial absorbance of the DNA/methyl green solution**

Table 10: TSC and its divalent (II) complexes on superoxide radicals generated by PMS/NADH system

Sample	Δ Through 5 min	%Inhibition
Control	0.420	0.00
L-Ascorbic acid	0.083	80.23
TSC	0.093	77.85
$[Co(TSC)(OAc)_2].3H_2O$	0.171	62.00
$[Ni_2(TSC\text{-}2H)(OAc)_2].2H_2O$	0.147	67.30
$[Cu_2(TSC\text{-}2H)(OAc)_2]$	0.400	11.10

Conclusion

In the present work, a novel thiosemicarbazide derivatives, 2,2'-(9,10-dihydro-9,10-ethanoanthracene-11,12-dicarbonyl) bis (N-allyl hydrazine-1-carbothioamide) (TSc) and its Co(II), Ni(II) and Cu (II) complexes were prepared and their structures were elucidated by elemental ,spectral, molar conductivity as well as thermogravimetric analysis methods. IR, UV-vis and magnetic moments measurements suggested an octahedral geometry for title complexes. Theoretical modelling using DFT method was carried out and the parameters withdrawn like bond lengths, bond angles, HOMO and LUMO in addition to some other energetic parameters such as softness, hardness, electronegativity and MEP map were evaluated. All revealed the great chemical reactivity and the significant biological activity and more electron donating ability of the thiosemicarbazide as revealed by the small energy band gap especially Cu (II) complex and Co(II) complex suggest that they can be complexes are semi-conductors and comprise of (E_{HOMO}-E_{LUMO}). Also the values of the energy band gap of investigated complexes.

The same variety of extremely efficient photovoltaic organic/inorganic complexes. The antioxidant activities including DNA binding and SOD-like activity revealed a potent good inhibitory activity displayed by the thiosemicarbazide ligand, TSC that is similar to the standard revealing the potent activity to intercalate DNA. This is referred to the availability of numerous active sites such as six secondary NH, two C=O, two thione groups as well as the planarity of the phenyl rings that can intercalates toward the minor groove the Cyt5 and Gua6. Further, according to data of SOD mimic activity assay, TSC (potent activity followed by Co(II) and Ni(II) complexes indicating that the synthesized compounds are good SOD mimic scavengers comparable to the standard drug, ascorbic acid. So, these compounds can be candidate for employing as antioxidant and anticancer drugs.

Disclosure statement

There are no conflicts to declare

References

[1] S. Pandeya, J. Dimmock, Recent evaluations of thiosemicarbazones and semicarbazones and related compounds for antineoplastic and anticonvulsant activities, Die Pharmazie, 48 (1993) 659-666.

[2] H.G. Petering, H.H. Buskirk, J.A. Crim, The effect of dietary mineral supplements of the rat on the antitumor activity of 3-ethoxy-2-oxobutyraldehyde bis (thiosemicarbazone), Cancer Res., 27 (1967) 1115-1121.

[3] D.R. McMillian, H.R. Engeseth, K.D. Karlin, J. Zubicta, Biological and Inorganic Copper Chemistry, Adenine Press, Guilderland, New York, (1986).

[4] E. Bouwman, W.L. Driessen, J. Reedijk, Model systems for type I copper proteins: structures of copper coordination compounds with thioether and azole-containing ligands, Coord. Chem. Rev., 104 (1990) 143-172.

[5] O.A. EL-Gammal, I.M. Abd Al-Gader, A.A. El-Asmy; Synthesis, characterization, biological activity of binuclear Co(II), Cu(II) and mononuclear Ni(II) complexes of bulky multi-dentate thiosemicarbazide"; Spectrochim. Acta Part A:128, (2014) 759–772.

[6] G.A. Gazieva, A. N. Kravchenko "Thiosemicarbazides in the synthesis of five- and six-membered heterocyclic compounds"; Russ. Chem. Rev., (2012) 81 (6) 494 – 523.

[7] S.E. Ghazy, O. A. El-Gammal, Dina A. Saad, A.A. El-Asmy "Flotation-Separation and Spectrophotometric Determination of Iron (III) in Natural Waters, Steel Samples and Pharmaceutical Formulation Using 1-(3,4dihydroxybenzlyidene)Thiosemicarbazide", Mans. J. Chem., (2008)35 (2).

[8] X. Zhang, P.lei, T. Sun, X. Jin, X. Yang, Y. Ling" Design, Synthesis, and Fungicidal Activity of Novel Thiosemicarbazide Derivatives Containing Piperidine Fragments "Molecules, (2017)22, 1-13.

[9] O. A. Al-Gammal, A. A. El-Asmy, " Synthesis and spectral characterization of 1-(aminoformyl- N -phenylform)-4-ethylthiosemicarbazide and its metal complexes" J. Coord. Chem., 61(2008), 2296.

[10] O.A. El-Gammal, G.M. Abu El-Reash, M.M. El-Gamil,"Binuclear copper(II), cobalt(II) and Nickel(II) complexes of N1-ethyl-N2-(pyridin-2-yl) hydrazine-1,2-bis(carbothioamide): Structural, spectral, pH-metric and biological studies" Spectrochim. Acta Part A:96 (2012), 444–455.

[11] D. Osman, A.Cooke, T. R. Young , E.Deery, N. J. Robinson, M. J. Warren "The requirement for cobalt in vitamin B12: A paradigm for protein metalation" Biochim. Biophys. Acta (BBA) - Molecular Cell Research, 1868(1) (2021), 118896-118941.

[12] Bao - Li Fei, W u - Shuang Xu, Hui - Wen Tao, Wen Li, Y u Zhang, Jian - Ying Long, Qing - B o Liu, Bing Xia, Wei - Yin Sun, Effects of copper ions on DNA binding and cytotoxic activity of a chiral salicylidene Schiff base, J. Photochem. Photobio.B Biol. 132 (2014) 36 -44.

[13] H.B. Kraatz, N. Metzler -Nolte, Concepts and Models in Bioinorganic Chemistry, Wiley -VCH: Weinheim, Germany (2006).

[14] S.J. Lippard, J.M. Berg, Principles of Bioinorganic Chemistry, University Science Books: Mill Valley, CA, (1994).

[15] J.J.R. Frausto da Silva, R.J.P. Williams, The Biological Chemistry of the Elements, Clarendon: Oxford, U. K. (1991).

[16] S. Labbe, D.J. Thiele, Pipes and wiring: the regulation of copper uptake and distribution in yeast, Trends Microbiol. 7 (1999) 500 -505.

[17] S. Medici, M. Peana, V.M. Nurchi, J.I. Lachowicz, G. Crisponi, M. A. Zoroddu, Noble metals in medicine: Latest advances, Coord. Chem. Rev. 284 (2015) 329 -350.

[18]K.Y.Djoko, C.Y.Ong, M.J.Walker, A.G.Mc Ewan" The Role of Copper and Zinc Toxicity in Innate Immune Defense against Bacterial Pathogens" J Biol Chem. 290(31) (2015) (31)18954–18961.

[19] U. Babu, M. L. Failla "Respiratory burst and candidacidal activity of peritoneal macrophages are impaired in copper-deficient rats". J. Nut. 120(1990), 1692–1699.

[20] O.A El-Gammal, M Gaber, SA Mandour "Novel VO (IV) complexes derived from a macrochelates: Synthesis, characterization, molecular modeling and in vivo insulin-mimic activity studies" J. App. Organomet. Chem.; (2020)34 (9), 5699.

[21] N. S. Burres, A. Frigo, R. R. Rasmussen, J. B. McAlpine, "A Colorimetric Microassay for the Detection of Agents that Interact with DNA" J. Nat. Prod. 1992, 55, 11, 1582–1587.

[22] O.A. El-Gammal, Sara A. El-Brashy, G. M. Abu El-Reach" Macrocyclic $Cr^{3+,}$ Mn^{2+} and Fe^{3+} complexes of a mimic SOD moiety: Design, structural aspects, DFT, XRD, optical properties and biological activity" App. Organomet. Chem. 5456 (2020),1-15

[23] B. Delley " Hardness conserving semilocal pseudopotentials" Phys. Rev. B Condens.Matter,66 (2002), 155125-155129.

[24] "Modeling and Simulation Solutions for Chemicals and Materials Research", Materials Studio, Version 7.0, Accelrys software Inc., San Diego, USA (2011).

[25] A.Matveev, M. Staufer,M. Mayer " Density functional study of small molecules and transition-metal carbonyls using revised PBE functionals"; Int. J. Quantum Chem. (1999), 75:863-873.

[26] O.A. El-Gammal, M.M. Bekheit and S.A. El-Brashy"Synthesis, characterization and in-vitro antimicrobial studies of Co (II), Ni (II) and Cu (II) complexes derived from macrocyclic compartmental Ligand" Spectrochim. Acta Part A:137, (2015) 207-219.

[27] O. A. El-Gammal, M.M. Bekheit, and Mai Tahoon"Synthesis, characterization and biological activity of 2-acetylpyridine- α-naphthoxyacetyl hydrazone (HA2PNA) and its metal complexes" Spectrochimica Acta Part A:135, (2015) 597-607.

[28] O.A. El-Gammal, G.M. Abu El-Reash, S.E. Ghazy, A.H. Radwan"Synthesis, characterization, molecular modeling and antioxidant activity of (1E, 5E)-1,5- bis(-pyridin-2-yl)ethylidene) carbohydrazide (H2APC) and its zinc(II) ,

cadmium(II) and mercury (II) complexes" J.Mol. Struct.1020 (2012) 6-15.

[29] O.A. El-Gammal, R.M. El-Shazly, F.E. El-Morsy, A.A. El-Asmy" Synthesis, characterization, molecular modeling and antibacterial activity of $N^{1/}$, $N^{2/}$-bis[1-(pyridin-2-yl) ethylidene] oxalohydrazide and its metal complexes" J. Mol. Struct. 998 (2011) 20.

[30] V. A. Tran , N. H. T. Tran, L. G. Bach , T. D. Nguyen, T. T. Nguyen, T. T. Nguyen , T. A. N. Nguyen , T. K. Vo, Thu-Thao T. Vo , V. T. Le "Facile Synthesis of Propranolol and Novel Derivatives" Hindawi J. Chem. Volume 2020, 1-12

[31] V. A. Tran, Thu-Thao T. Vo, My-Nuong, T. Nguyen, N. D. Dat, Van-Dat Doan, Thanh-Quang Nguyen, Q.H. Vu, V.T. Le, T. D. Tong" Novel α-Mangostin Derivatives from Mangosteen (Garcinia mangostana L.) Peel Extract with Antioxidant and Anticancer Potential" Volume 2021, Article ID 9985604, 12 pages" Hindawi J. Chem. Volume 2021, 1-12.

[32] O.A. El-Gammal and M.M. Mostafa "Synthesis, characterization and molecular modeling of Girard′Tthiosemicarbazide and its complexes with some transition metal ions" Spectrochim. Acta. Part A: (2014) 530- 542.

[33] M.R. Mlahi, O.A. El-Gammal, M.H. Abdel-Rahman, I.M. Abd Elkader" Synthesis, characterization, DFT molecular modeling and biological studies of Zn(II), Cd(II) and Hg(II) complexes of new polydentate thiosemicarbazide"J.Mol. Struct,1182(2019)168-180.

[34] O.A.El-Gammal, El-Sayed A.Elmorsy and Y. E.sherif,"Evaluation of the anti-inflammatory and analgesic effects of Cu(II) and Zn(II) complexes derivedfrom2-(naphthalen-1-yloxy)-N'-(1-(pyridin-2-yl) ethylidene) acetohydrazide" Spectrochim. Acta part A:120 (2014) 332-339.

[35] O.A.El-Gammal, D.A.Saad, A.F.Al-Hossainy"Synthesis, spectral characterization, optical properties and X-ray structural studies of S centrosymmetric N_2S_2 or $N_2S_2O_2$ donor Schiff base ligand and its binuclear transition metal complexes" J. Mol. Struct. 1244 (2021) 130974.

[36] A. W. Coats, J. P. Redfern," Kinetic parameters from thermogravimetric data, Nature, 201 (1964) 68-69.

[37] H. Horowitz, G. Metzger" A new analysis of thermogravimetric traces", Anal. Chem. 35 (1964) 1464-1468.

[38] O. A. El-Gammal, F. Sh.Mohamed, G.N.Rezk, A. A. El-Bindary" "Synthesis,characterization, catalytic, DNA binding and antibacterial activities of Co(II),Ni(II) and Cu(II) complexes with new Schiff base ligand "J.Mol.Liq. 326(2021) 115223.

[39] O. A. El-Gammal, F. Sh. Mohamed, G.N. Rezk, A. A. El-Bindary" Structural characterization and biological activity of a new metal complexes based of Schiff base" J. Mol. Liq.330 (2021), 115522.

[40] O.A. El-Gammal, E. Abdel-Latif, M. G. Farag, M. H. Abdel-Rahman" Synthesis, characterization, and anticancer activity of new binuclear complexes of 2,20 -malonylbis(N-phenylhydrazine-1-carbothioamide"J.App.Organomet. Chem.35 (2021):e6194.

[41]V.A. Tran, L. T.N. Quynh, Thu-ThaoT. Vo, P. A.Nguyen, T. N.Don, Y.Vasseghian, H.Phan, S ang-W. Lee"Experimental and computational investigation of a green Knoevenagel condensation catalyzed by zeolitic imidazolate framework-8" Env. Res. 204 D (2022) 112364.

[42] V.A. Tran K. B.Vu, Thu-ThaoT. Vo, V.T. Le, H. H.Do, L. G.Bach, Sang-Wha Lee "Experimental and computational investigation on interaction mechanism of Rhodamine B adsorption and photodegradation by zeolite imidazole frameworks-8" Applied Surface Science, 538(2021), 148065.

[43] O.A. El-Gammal "Synthesis, Characterization and Antimicrobial Activity of 2-(2-ethylcarbamothioyl) hydrazinyl) 2-oxo-N-phenylacetamide copper complexes" Spectrochim Acta Part A., 75(2010) 533.

[44] O. A. El-Gammal , A. A. El-Bindary, F. Sh.Mohamed, G.N.Rezk, M. A. El-Bindary "Synthesis, characterization, de, sign, molecular docking, anti-COVID-19 activity, DFT calculations of novel Schiff base with some transition metal complexes" J. Mol. Liq. (2021) 117850.

[45] K.Chavva, S.Pillalamarria, V.Bandaa, S.Gauthama, J.Gaddamedia, P.Yedla, C.G.Kumar, N.Banda" Synthesis and biological evaluation of novel alkyl amide functionalized trifluoromethyl substituted pyrazolo[3,4-b]pyridine derivatives as potential anticancer agents" Bioorg.& Med. Chem. Let. 23(21)(2013), 5893-5895.

[46] Z. A. Siddiqi, P.K. Sharma, M. Shahid, M. K. Anjuli. , A. Siddique , S. Kumar" Superoxide scavenging and antimicrobial activities of novel transition metal complexes of oxydiacetate dianion as primary ligand: Spectral characterization, cyclic voltametric investigations and crystal structure; Eur. J. Med.Chem.; 57, (2012) 102-111